Simulation of energy impact of an energy recovery ventilator in Northern housing

Jing Li, Radu Zmeureanu, and Hua Ge

Centre for Zero Building Energy Studies, Department of Building, Civil and Environmental Engineering, Gina Cody School of Engineering and Computer Science, Concordia University, Montreal, Qc, Canada

Abstract: The single core Energy Recovery Ventilator (ERV) used in this study is equipped with defrost control that recirculates the exhaust indoor air, while keeps the outdoor air intake damper closed. This defrost strategy has the disadvantage of reducing the outdoor air supplied to the house, which may affect the indoor air quality. First, this paper presents new correlation-based models of supply air temperature T_2 after the energy recovery core during normal and defrost operation modes based on laboratory experimental data. A pre-heating coil heats the supply air from T_2 to indoor air temperature. Second, a house in Montreal (4356 HDD) is simulated as a reference using TRNSYS program. Since the program cannot simulate the operation under defrost mode, the new models are connected in TRNSYS using equation boxes. The energy use of houses at three locations in northern Canada with HDD of 8798 (Inuvik), 8888 (Kuujjuaq) and 12208 (Resolute), are also simulated, without and with ERV unit. The seasonal energy used for heating the house and pre-heating the supply air is compared with results from Montreal. Compared to the case without heat recovery, the ERV unit leads to energy savings: 24% (Montreal), 26% (Inuvik), 27% (Kuujjuaq), and 27% (Resolute). Compared to the minimum standard requirements, the outdoor airflow rate due to defrost is reduced by 4.7% (223 hours) in Montreal, 19% (1043 hours) in Inuvik, 13% (701 hours) in Kuujjuaq, and 24% (1379 hours) in Resolute.

1. Introduction

Reducing energy consumption in buildings plays an important role in reducing CO_2 emissions since the building sector accounts for 40% of the global energy use [1]. New houses with higher airtightness and energy efficiency (R-2000-certified houses) have been increasingly constructed to reduce heat losses and their energy impacts during operation [2]. For relatively cold climates, to ensure air quality and thermal comfort as well as reduce energy use, finding the optimal mechanical ventilation solution is the concern in residential well-insulated buildings [3]. Energy use in ventilation systems without heat/energy recovery is significant in cold climates. To make a further reduction in energy use possible, it is essential to focus on high energy efficient ventilation and heat/energy recovery system [4].

The membrane energy exchanger (MEE) is recommended for cold climate applications because of its better performance on the frost-resistance and energy saving than other types of heat/energy exchangers applied to cold climates [5-7]. The formation of frost in the energy recovery ventilator (ERV) is the primary concern for the operation in cold climates. The frost occurs inside a membrane-based ERV when the outdoor air temperature is between -8°C and -12°C. The airflow rate of warm exhaust air entering the exchanger is reduced. As a result, the thermal efficiency of the unit diminishes, and the unit can be damaged if no measurements are taken to remove the frost [8-10].

Some publications [11-16] focused on the development of frost protection techniques and defrosting methods for the air-to-air heat/energy exchangers over the past 30 years in order to maintain high energy recovery effectiveness. Preheating the outdoor air, bypassing the outdoor airflow, reducing the supply airflow rate, and recirculating warm exhaust air have proved to be effective methods for the protection of exchangers [11,13]. The exhaust air recirculation was found to be the most appropriate for extremely cold climates [17]. When frost formation within the exchanger core reaches a critical level, the unit stops the supply of outside air, and the exhaust air is recirculated through the exchanger core to melt the accumulated frost.

HRV/ERV coupled with the recirculation defrost was widely investigated by laboratory-based experiments [8,14,18-20, 23]. However, to our knowledge, there are no publications on the analysis of HRV/ERV with the recirculation defrost, numerically or experimentally, for extremely cold climates.

The main objective of this paper is to evaluate the effect of recirculation defrost in ERV on: the total energy use of the house, the energy use for pre-heating outdoor air, the reliability of ERV in supplying the required outdoor air, and the effect on indoor humidity.

*Jing Li: 052312quph@gmail.com; Radu Zmeureanu: radu.zmeureanu@concordia.com; Hua Ge: hua.ge@concordia.com

For this purpose, correlation-based ERV models are developed based on laboratory experimental data [8], and added to the energy model developed in TRNSYS for a Net-zero Energy house (NZEH) in Montreal [21]. This model is used for the analysis of single-core ERV using the manufacturer's recirculation defrost schedule. The study includes also the assessment of this defrost method at three northern Canadian locations.

2. Methodology

2.1. NZEH house model

The NZEH model, developed in Type 56 in TRNSYS, is for a two-storey house with a ventilated attic and a basement. The house is divided into five zones including Zone A1/basement ($41.23 m^2$), ground floor Zone B1^w ($41.23 m^2$), plus Zone B1^e ($42.37 m^2$), second floor Zone C1 ($83.58 m^2$), and unheated zones of a garage ($42.4 m^2$) and attic ($83.6 m^2$). The setpoint operative temperature of all heated zones is 22℃. Some features of the building envelope of the NZEH house model are presented in **Table 1**, while HVAC features in **Table 2.**

Table 1: Building envelope features of the NZEH house model

Features	Technical information
Building heated floor area	334 m²
Occupancy	Two adults and three children
Above ground walls	RSI-6.25 (m²·K/W)
Basement walls	RSI-2.47 (m²·K/W)
Roof	RSI-10.42 (m²·K/W)
Basement floor	RSI-1.90 (m²·K/W)
Windows	RSI-1.90 (m²·K/W)
Natural Air Infiltration	0.061 ACH
(airtightness)	1.22 ACH at 50 Pa

Note: Tables shows the effective thermal resistance of building envelope components

Table 2: Features of the HVAC system of NZEH house model [21]

Equipment	Technical information
Space Heating	Hydronic radiant floor heating with an electric heaters and water storage tank (Type 534)
ERV	Apparent sensible efficiency of 67% at 57 L/s and 0℃ outdoor air temperature; 46% latent recovery efficiency at 57 L/s and 0 ℃ outdoor air temperature
Defrost	7 min defrost and 25 min operation between -10 to -27℃; and 10 min defrost and 22 min at outdoor air temperature lower than -27℃

### 2.2. Development and verification of ERV unit models during the normal and defrost operation

The supply air temperature T_2 that leaves the ERV varies with the outdoor air temperature $T_1 = T_{outdoor}$, and the defrost/frost operation regime. The supply air temperature T_5 that enters the house is kept constant at $T_5 = T_{indoor}$, being controlled by the heating coil (HC), installed after the ERV (**Figure 1**). During the defrost by recirculation, the outlet of exhaust air and inlet of supply outdoor air are closed. The exhaust air from the house that enters the ERV unit is recirculated through the channels of the unit, and then enters the heating coil

(HC) before being supplied to the house. The indoor air quality (IAQ) of the house is affected during the recirculation defrost because the stale exhausted air is reintroduced into the house; there is no outdoor air introduced into the house during the defrost operation.
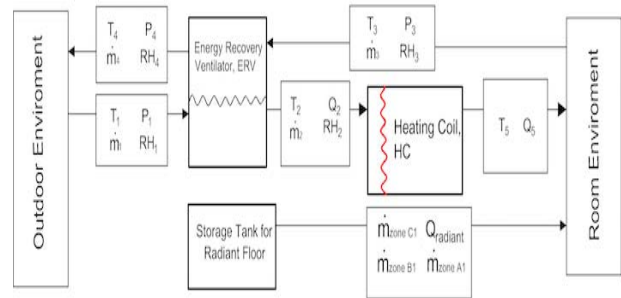
Figure 1: Schematic representation of air-to-air energy recovery system

The estimation of electric power input to heating coil, which is used to increase the temperature of outdoor air stream from T_2 to T_5, is needed for the overall estimation of the energy demand of the house during the heating season. The duration of normal and defrost operation modes is set according to manufacturer's specification (**Figure 2**).
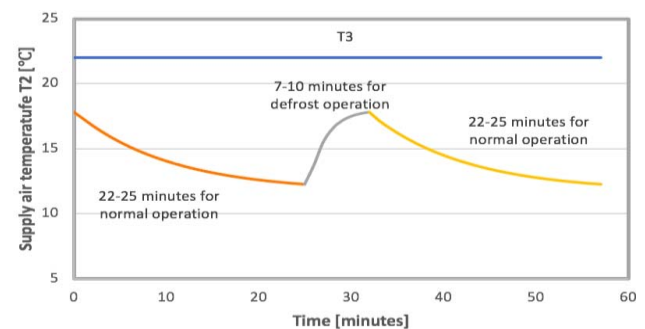
Figure 2: Schematic variation of supply air temperature T_2 of the single core ERV operation over time at T_1=-20℃ and T_3=22℃.

2.2.1. Development of correlation-based models of supply air temperature T_2 during normal operation

The frosting effect on the supply air temperature T_2 of energy recovery unit is not considered in the built-in energy recovery component in TRNSYS. Therefore, it is needed to develop different correlation-based models of supply air temperature during the normal operation and defrost operation, respectively.

A series of correlation-based models that predict the supply air temperature T_2 versus time t at different outdoor air temperatures T_1 are developed (**Table 3**) based on Beattie's experimental results (**Figure 3**) [8]. Data points for T_1 = -10ºC and -15ºC almost overlap. These models consider the effect of frost on the heat exchange process, if the frost occurs in the exhaust air channel. The correlation-based models of supply air temperature T_2 are written in the equation components of TRNSYS and integrated in the house model.

Table 3: Correlation-based models of supply air temperature T_2 with respect to time t for the first 30 minutes of normal operation

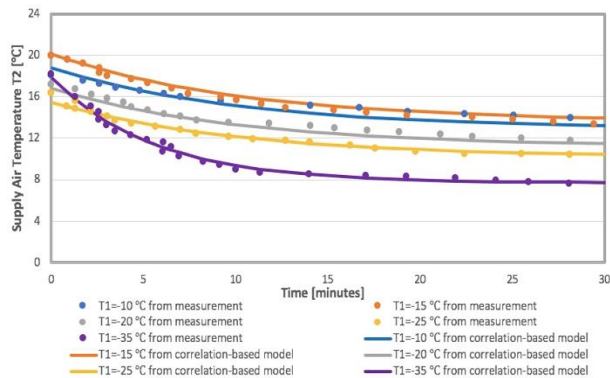| T_1 [°C]	Correlation-based model	R^2 [-]
-10	$T_2=0.263 \cdot T_{2(t=0)} \cdot (1-e^{-0.0722t})+18.001$	0.99
-15	$T_2=0.397 \cdot T_{2(t=0)} \cdot (1-e^{-0.094t})+20.044$	0.99
-20	$T_2=0.316 \cdot T_{2(t=0)} \cdot (1-e^{-0.101t})+17.188$	0.99
-25	$T_2=0.319 \cdot T_{2(t=0)} \cdot (1-e^{-0.113t})+15.869$	0.99
-35	$T_2=0.586 \cdot T_{2(t=0)} \cdot (1-e^{-0.19t})+18.242$	0.99

Where $T_{2(t=0)}$ is the air temperature leaving the heat recovery unit at the beginning of the normal operation, which is equal to air temperature T_2 at the end of the defrost operation.

If the outdoor air temperature T_1 is different from the values listed in **Table 3**, a linear interpolation is used between the closest correlation models. For instance, if the outdoor air temperature is T_1 = -12.5°C, the interpolation is made between the values of -10°C and -15°C at every time step t.

To avoid the interpolation, the outdoor air temperature T_1 needs to be included in the correlation-based model. **Equation 1** presents one single correlation-based model for the prediction of supply air temperature T_2, developed in terms of time t and outdoor air temperature T_1 from measurements of reference [8].

$$T_2= T_{2(t=0)} \cdot [A \cdot T_1 - B \cdot (1 - e^{-Ct}) + D] \qquad (1)$$

Equation 1 corresponds to the specific ERV unit used in [8]. The coefficients of fitting curve are determined from measurements as follows: A=0.006 B=0.328, C=0.097, and D=1.102 (**Figure 3**) at -10°C, -15°C , -20°C and -25°C; and A=0.004, B=0.559, C=0.18 and D=1.126 at -35°C. The predicted supply air temperature T_2 (**Equation 1**) agrees well with the measurements of supply air temperature T_2 as the coefficient of determination R^2 has values between 0.96 and 0.99. Therefore, the supply air temperature T_2 can be calculated with **Equation 1** to avoid the interpolation using equations listed in **Table 3**.

Figure 3: Measured and predicted supply air temperature T_2 at different outdoor air temperatures during normal operation

2.2.2. Development of correlation-based models of supply air temperature T_2 during defrost operation

When defrost is required, the supply air inlet damper and exhaust air outlet damper are closed. The airflow is recirculated from the exhaust air inlet to the supply air outlet. The ERV (**Type 667b**) in TRNSYS does not take into account the melting effect in the ERV on the supply air temperature T_2. Therefore, correlation-based models of supply air temperature T_2 during the defrost operation are developed using available measurements from [8]. The following data points are available: (i) at the beginning of defrost, and (ii) at the end of defrost (**Table 4**).

Table 4: Supply air temperature T_2 at the beginning and end of defrost operation [8]

T_1 [°C]	Inlet T_3 [°C]	T_2 at the beginning of defrost operation [°C]	T_2 at the end of defrost operation [°C]
-10	21.7	14.1	18
-15	21.7	13.8	18
-20	21.7	12	18
-25	21.7	10.45	18
-35	21.7	8	18

The supply air temperature T_2 during the defrosting period is modelled with **Equation 2,** which represents the general pattern of variation as presented in [6] from detailed measurements at 5 s time intervals.

$$T_2 =A \cdot (T_{2 (t=0)} +(T_{2 (t=7 \, or \, 10)} - T_{2 (t=0)}) \cdot (1-e^{-B \cdot t})) \qquad (2)$$

Where T_2 is the supply air temperature [°C]; $T_{2 (t=0)}$ is the supply air temperature [°C] at the beginning of defrost (**Table 4**); A and B are coefficients to be determined; $T_{2 (t=7 \, or \, 10)}$ is the supply air temperature at the end of defrost (**Table 4**); and t is the time during defrost [minutes]. The correlation-based models of supply air temperature developed by **Equation 2** at different outdoor temperatures are listed in **Table 5**, and the predicted supply air temperature T_2 during the defrost operation is presented in **Figure 4.**

Table 5: The correlation-based model of supply air temperature T_2 at different outdoor air temperature T_1 versus time t during the defrost regime of 7 minutes and 10 minutes

T_1 [°C]	Correlation-based model	
-10	$T_2 =1.0068 [14.1 +(18-14.1) \cdot (1-e^{-0.5t})$	$0< t < 7$minutes
-15	$T_2 =1.007 [13.8 +(18-13.8) \cdot (1-e^{-0.5t})]$	$0< t < 7$minutes
-20	$T_2 = 1.01[12 +(18-12) \cdot (1-e^{-0.5t})]$	$0< t < 7$minutes
-25	$T_2 =1.013 [10.45 +(18-10.45) \cdot (1-e^{-0.5t})]$	$0< t < 7$minutes
-35	$T_2 =1.0035 [8 +(18-8) \cdot (1-e^{-0.5t})]$	$0< t < 10$minutes

The supply air temperature T_2 is obtained by interpolating between the correlation-based models when the outdoor air temperature T_1 is not listed in **Table 5**.

To avoid the interpolation, the outdoor air temperature T_1 is included in the correlation-based model of supply air temperature T_2, developed in terms of time t and outdoor temperature T_1 (**Equations 3 and 4**).

$$T_2 =AT_1 + T_{2 (t=0)} +(T_{2 (t=7 \, or 10)} - T_{2 (t=0)}) \cdot (1-e^{-Bt}) \qquad (3)$$

Where:

$$T_{2 (t=0)} =0.2497 \, T_1 + 17.124 \qquad (4)$$

Equations 3 and 4 corresponds to the specific ERV unit used in [8]. The coefficients of fitting curve (**Equation 3**) are determined from measurements as follows: A = 0.0, and B = 0.533. The predicted supply air temperature T_2 (**Figure 4**) agrees well with the supply air temperature T_2 **in Table 5** as the coefficient of determination R^2 has values of around 0.99.
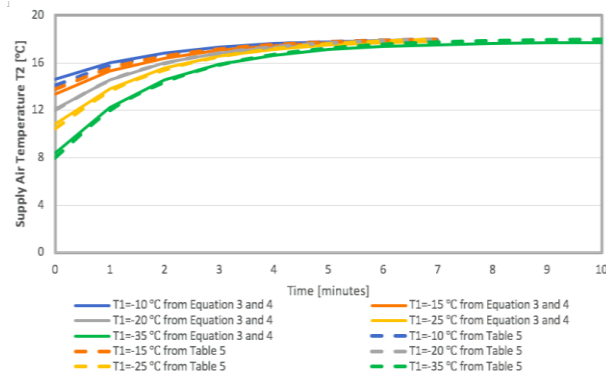
Figure 4: Predicted supply air temperature from **Table 5** and predicted supply air temperature T_2 by **Equations 3 and 4** at different outdoor air temperatures during defrost operation

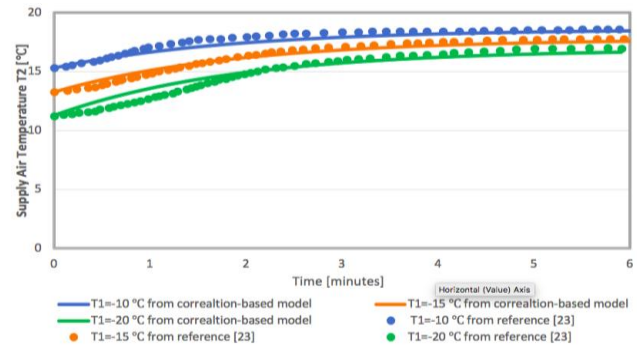### 2.2.3. *Verification of correlation-based models for the normal and defrost operation*

The verification of correlation-based models for the normal and defrost operations is made by comparing with measurements from reference [23] under the same initial supply air temperature when the outdoor air temperature T_1 =-20℃ (**Figure 5**).
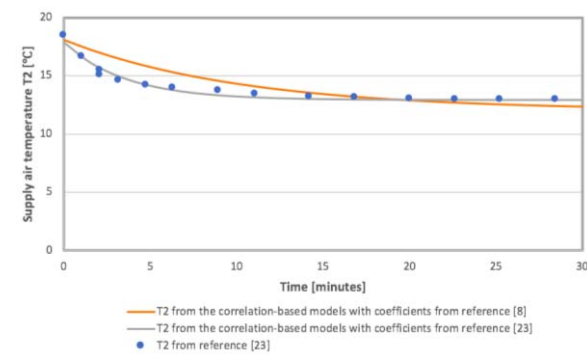
Figure 5: Comparison of predicted supply air temperature T_2 from the correlation-based models with the coeffecients based on reference [8] and reference [23] during normal operation and experimental results from reference [23] at outdoor air temperature of -20 ℃

The pattern of variation is quite similar, and the coefficient of determination is R^2=0.78 (**Figure 5**). The difference is greater during the first 10 min of normal operation, which may be attributed to the different physical characteristics of ERVs used by [8] and [23]. The correlation-based model with the coefficients (A=1.352E-05, B=0.265, C=0.28 and D=0.965), determined from data [23], has better prediction results with R^2 = 0.95 when compared to measurements from [23] (**Figure 5**).

Supply air temperature T_2 is calculated for the defrost operation with the correlation-based model (**Equations 3 and 4**) and coefficients A=0.0 and B=0.525, determined based on data from [23] at several outdoor air temperatures T_1. As shown in **Figure 6**, these predictions agree well with measurements with $R^2 = 0.97\text{-}0.99$.

Figure 6: Comparison of predicted supply air temperature T_2 using **Equations 3** and **4** with the data from reference [23] during the defrost operation against measurements from reference [23].

2.3. **Development of correlation-based models of supply air humidity w_2 of normal and defrost operation**

Moisture transfer between the outdoor air and exhaust air only occurs in the ERV unit. There is no change in the humidity ratio through the heatng coil ($w_2 = w_5$) (**Figure 1**). The supply air humidity ratio w_2, leaving the ERV unit, decreases during the 22-25 min of normal operation, then increases during the 7-10 min defrost operation. After the defrost operation, the cycle of normal and defrost operations is repeated (**Figure 7**), where w1 is outdoor humidity ratio and w3 is inlet exhaust humidity ratio.
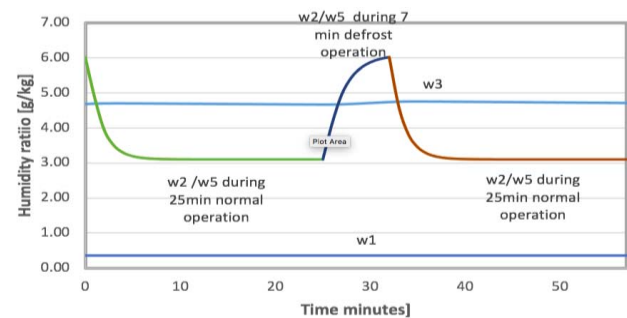
**Figure 7:** Schematic variation of supply air humidity w_2 of the conventional single core operation with time at T_1=-20℃ and w_1=0.36g/kg

2.3.1. *Development of correlation-based models of supply air humidity ratio w_2 of normal operation*

The frosting effect on the supply air humidity w_2 of ERVis not considered in the built-in energy recovery component in TRNSYS. Therefore, there is a need for developing different correlation-based models of supply

air humidity ratio w_2 during the normal operation and defrost operation, respectively.

Beattie's experimental results at -25 °C and -35 °C of outdoor temperature (**Figure 8**) [8] are used to obtain the results for the other specific outdoor temperature (-10°C, -15°C and -20°C) (**Figure 8**). The effect of frost on the heat exchange process is taken into consideration in these models. The correlation-based models of supply air humidity ratio w_2 written in the equation components of TRNSYS are integrated in the house model when the frost occurs in the indoor air exhaust channel, while the built-in energy recovery component (**Type 667**) in TRNSYS is utilized when the frosting does not occur.
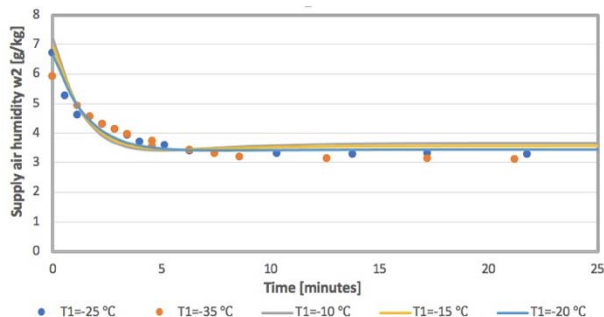

Figure 8: Supply air humidity w_2 of ERV unit at T_1=-10°C, -15°C and -20°C versus time during normal operation and suppy air humidity w_2 at T_1=-25°C, -35°C by experiment [8].

Equation 5 predicts the supply air humidity w_2, in terms of time t and outdoor air temperature T_1 from measurements of reference [8].

$$w_2 = w_{2(t=0)} \cdot [A \cdot T_1 \text{-} B \cdot (1 - e^{-Ct}) + D] \qquad (5)$$

Where $w_{2(t=0)}$ is the supply air humidity leaving the ERV at the beginning of the normal operation, which is equal to supply air humidity w_2 at the end of the defrost operation: A, B, C and D are coefficients to be determined and t is the time during the normal operation, from 0 to 25 minutes. **Equation 5** corresponds to the specific ERV unit used in [8]. The coefficients of the fitting curve (**Equation 5**) are determined from measurements as follows: A=0, B=0.448, C=0.738, and D=0.96 at -10°C, -15°C , -20°C and -25°C and A=0.005, B=0.47, C=0.363 and D=1.16 at -35°C As shown in **Figure 9**, the predicted supply air humidity w_2 using **Equation 5** are in good agreement with the measurements with the coefficient of determination R^2 between 0.96 and 0.99. Therefore, the supply air humidity w_2 can be calculated with **Equation 5**.
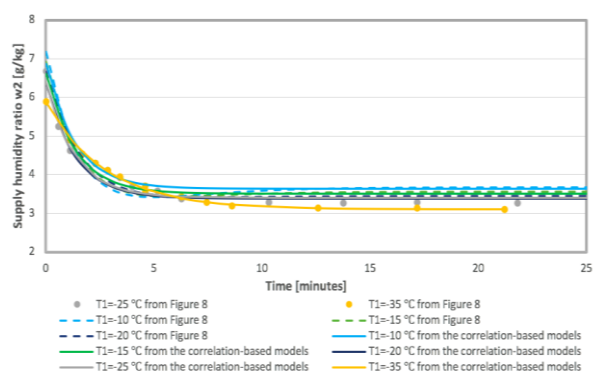
Figure 9: Measured and predicted supply air humidity w_2 from **Figure 8** and predicted supply humidity w_2 from the correlation-based models at different outdoor air temperatures during normal operation.

2.3.2. *Development of correlation-based models of supply air humidity w_2 of defrost operation*

The ERV (Type 667b) in TRNSYS does not consider the melting effect on the supply humidity w_2. Therefore, correlation-based models of supply air humidity w_2 during the defrost operation are developed based on available measurements from [8]. The following data points are available: (i) at the beginning of defrost, and (ii) at the end of defrost (**Table 6**). T_1 refers to the conditions at the end of normal operation, which influences the core temperature at the beginning of defrost by recirculation.

Table 6: Supply air humidity w_2 at the beginning and end of the defrost operation [8]

T_1 [°C]	w_3 [g/kg]	w_2 at the beginning of defrost operation [g/kg]	w_2 at the end of defrost operation [g/kg]
-10	5.44	3.74	6.1
-15	5.44	3.63	6.1
-20	5.44	3.46	6.1
-25	5.44	3.20	6.1
-35	5.44	2.75	6.1

The supply air humidity ratio w_2 during the defrosting period is modelled with (**Equation 6**), which represents the general pattern of variation as presented in [23] from detailed measurements at 5 s time intervals.

$$w_2 = A \cdot (w_{2(t=0)} + (w_{2(t=7 \, or \, 10)} - w_{2(t=0)}) \cdot (1 - e^{-B \cdot t})) \qquad (6)$$

Where $w_{2(t=0)}$ is the supply air humidity [g/kg] at the beginning of defrost (**Table 6**); A and B are coefficients to be determined; $w_{2(t=7 \, or \, 10)}$ is the supply air humidity w_2 at the end of defrost (**Table 6**); and t is the time during defrost [minutes]. The correlation-based models of supply air humidity w_2 developed by **Equation 6** are listed in **Table 7**, and the predicted supply air humidity w_2 during the defrost operation is presented in **Figure 12.**

Table 7: Correlation-based model of supply air humidity w_2 at different outdoor air temperatures T_1 versus time t during the defrost regime of 7 minutes and 10 minutes

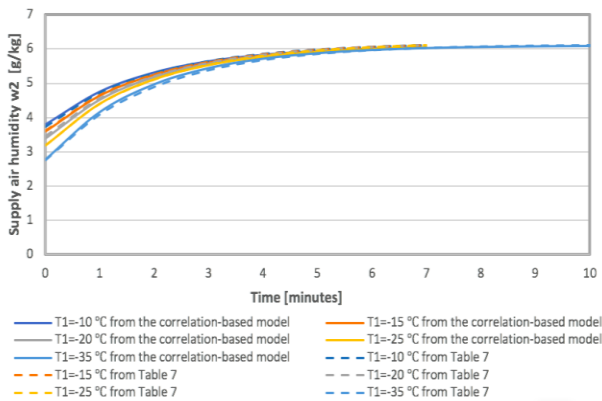| T_1 [°C]	Correlation-based model
-10	$w_2 = 1.012 (3.74 + (6.1-3.74)\cdot(1-e^{-0.5t}))$ $0 < t < 7$ minutes
-15	$w_2 = 1.0127 (3.63 + (6.1-3.63)\cdot(1-e^{-0.5t}))$ $0 < t < 7$ minutes
-20	$w_2 = 1.014(3.46 + (6.1-3.2)\cdot(1-e^{-0.5t}))$ $0 < t < 7$ minutes
-25	$w_2 = 1.015 (2.75 + (6.1-2.75)\cdot(1-e^{-0.5t})$ $0 < t < 7$ minutes
-35	$w_2 = 1.004 (8 + (6.1-8)\cdot(1-e^{-0.5t}))$. $0 < t < 10$ minutes

For conditions that are different from those in **Table 7**, interpolation can be used. To avoid the interpolation, one single model for the prediction of supply air humidity w_2 is developed with respect to time t and outdoor air humidity w_2 (**Equations 7 and 8**).

$$w_2 = AT_1 + w_{2\,(t=0)} + (w_{2\,(t=7\,or10)} - w_{2\,(t=0)}) \cdot (1 - e^{-Bt}) \quad (7)$$

Where:

$$w_{2\,(t=0)} = 0.0409\, T_1 + 4.2133 \quad (8)$$

Equations 7 and 8 corresponds to the specific ERV unit used in [8]. The coefficients of fitting curve (**Equation 7**) are determined from measurements as follows: A = 0.0, and B = 0.539. As shown in **Figure 10**, the predicted supply air humidity ratio w_2 agrees well with values obtained by equations of **Table 7**, with the coefficient of determination R^2 of around 0.99.

Figure 10: Predicted supply air humidity ratio w_2 in **Table 7** and predicted w_2 by **Equations 7 and 8** at diffrent w_1

2.3.3. *Verification of correlation-based models for the normal and defrost operations*

The verification of correlation-based models for the normal and defrost operations is made by comparing the predicted supply air humidity w_2 with measurements from reference [23] under the same initial supply air temperature when the outdoor air temperature T_1 = -20°C (**Figure 11**).
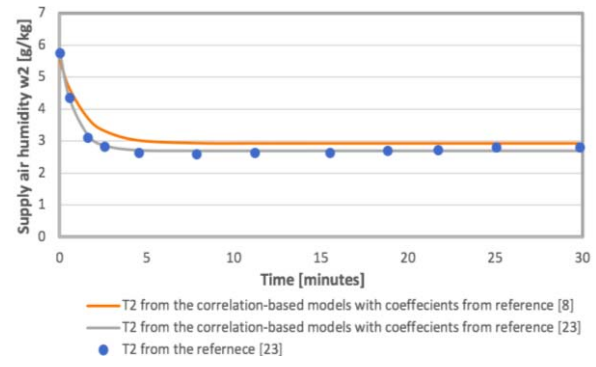
Figure 11: Comparison of predicted supply air humidity w_2 from the correlation-based models during normal operation and experimental results of reference [23] at outdoor air temperature of -20°C

The pattern of variation is quite similar, and the coefficient of determination R^2=0.96 (**Figure 11**). The difference is greater during the first 10 min of normal operation possibly as the results of the different physical characteristics for ERVs used by [8] and [23]. When the coefficients of **Equation 5** are obtained from data of [23], the agreement is better with R^2 = 0.99 when compared to measurements of [23] (**Figure 11**).

Supply air humidity w_2 is calculated for the defrost operation with the correlation-based model (**Equations 7 and 8**) and coefficients A = 0.0 and B = 1.16489 that are obtained from data of [23] at -20°C of outdoor air temperatures. As shown in **Figure 12**, the predicted supply air humidity w_2 is in good agreement with the experimental results from [23] with $R^2 = 0.99$.
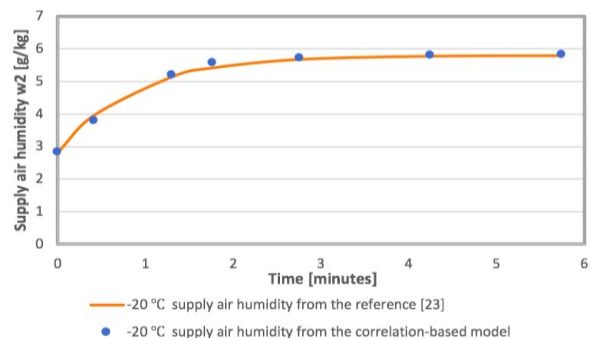
Figure 12: Measured and predicted supply air humidity w_2 using data from reference [23] during the defrost operation

3. Simulation results and analysis

The effect of single core operation of ERV unit on the energy use of the NZEH house model is evaluated for three arctic locations (Inuvik, Kuujjuaq and Resolute) and Montreal. The heating season is defined as follows: from October 17 to May 1 (Montreal), from September 5 to June 4 (Kuujjuaq and Inuvik), and the entire year (Resolute).

As an example, this section presents the simulation of energy use of NZEH house model located in Inuvik, using the ERV unit with the manufacture's defrost schedule. The total annual energy use for space heating of the NZEH house is 30,710.34 kWh, which is not affected by the ventilation heating by the heating coil (**Table 8**). Without the ERV unit, the ventilation heating

of the heating coil uses 14,863.22 kWh, which is reduced by 77% by the use of ERV. A summary of energy uses and defrost hours for all four locations are provided in **Table 9.** In general, the introduction of the ERV unit made a significant contribution to the total heating demand reduction of the NZEH house, ranging from 23% in Montreal to 25.17% in Inuvik. The ERV unit used in NZEH leads to greater ventilation heating energy savings (heating coil) under the arctic climate (from 75% to 79% in Kuujjuaq, Resolute and Inuvik) than in the cold climate of Montreal with 73% savings. Compared to the minimum standard requirements, the outdoor airflow rate due to defrost is reduced by 4.7% (223 hours) in Montreal, 19% (1043 hours) in Inuvik, 13%

(701 hours) in Kuujjuaq, and 24% (1379 hours) in Resolute. The radiant heating energy uses per heated floor for the entire heating season are 74.8 kWh/m^2 in Montreal, 147.64 kWh/m^2 in Inuvik, 127.76 kWh/m^2 in Kuujuaq and 202.7 kwh/m^2 in Resolute. **Figure 13** presents the house humidity ratio (average) with and without ERV. It can be seen that due to the moisture exchange inside the ERV unit and moisture from the melted ice during the defrost operation, the house humidity ratio increased in all four locations (Montreal, Inuvik, Kuujjuaq and Resolute) when comparing with the case without ERV, e.g., the average humidity ratio in Jan in Inuvik increased from 1.7g/kg to 4.9 g/k.

Table 8: Total annual energy consumption (ventilation heating by heatng coil and space heating) of the NZEH house in case with and without ERV unit in Inuvik

		With ERV unit			Without ERV unit			
Months	Defrost hours	Radiant heating (kWh)	Ventilaion heating by heating coil (kWh)	Total heating (kWh)	Radiant heating (kWh)	Ventilaion heating by heating coil (kWh)	Total heating (kWh)	Total energy savings (kWh)
Sep.	0	1631	233	1865	1631	761	2392	527
Oct.	57.73	2861	354	3216	2861	1364	4225	1009
Nov.	162.52	3731	392	4124	3731	1840	5572	1447
Dec.	191.41	4301	449	4751	4301	2118	6420	1668
Jan.	191.79	4517	458	4975	4517	2219	6736	1760
Feb.	169.51	4019	414	4434	4019	1979	5998	1564
Mar.	175.49	4149	429	4579	4149	2032	6181	1602
Apr.	93.48	3233	350	3583	3233	1507	4740	1156
May.	1.11	2169	283	2452	2169	964	3134	681
June	0	174	21	196.11	174	75	250	54
Total	1043.06	30710	3389	34099	30710	14863	45573	11473

Table 9: The comparison of the energy consumptions (ventilation heating by heatng coil and space heating) and defrost hours under three arctic climate (Kuujjuaq, Resolute and Inuvik) and one cold climate (Montreal) in the NZEH house

		With the ERV unit			Without ERV unit	
Locations	Radiant heating demand (kWh)	Ventilation heating demand (kWh)	Total heating demand (kWh)	Defrost frequency (hours)	Ventilation heating demand (kWh)	Total heating demand (kWh)
Montreal	15566	1938	17504	223.35	7172	22739
Resolute	42163	4794	46958	1379.08	20163	62326
Inuvik	30710	3389	34099	1043	14863	45573
Kuujuaq	26574	3087	29661	702.5	12599	39173
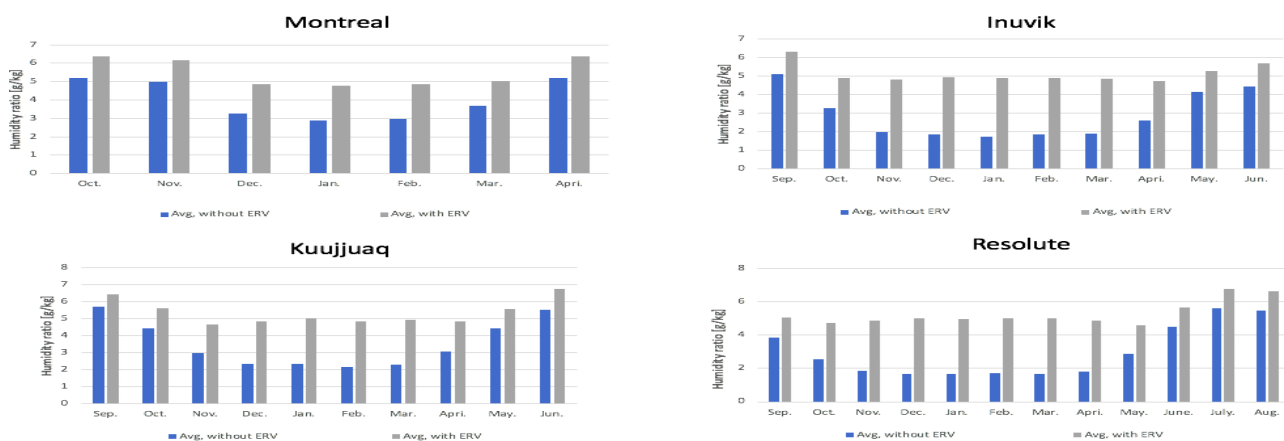
Figure 13: House humidity ratio with and without ERV unit during the heating season.

4. Conclusion

The ERV combined with recirculation defrost has been recognized as the most adequate ventilation strategy in extremely cold climates. To overcome the limits of the existing models (Type 667b) of the ERV unit in TRNSYS, the correlation-based models of supply air

temperature and humidity ratio of the ERV unit during the normal and defrost operation are developed by taking into account the effect of frosting and defrosting. The energy impact of the ERV unit with the recirculation

defrost on the NZEH house is investigated by integrating the correlation-based models into TRNSYS. Four cities are selected, three (Inuvik, Kuujjuaq and Resolute) located in the extremely cold climate and one (Montreal) in a cold climate as reference.. Compared with the case without the ERV unit, the ERV unit can significantly reduce the heating demand of the house for all locations, with Inuvik having the highest energy saving by 25.7%. The ERV unit makes a considerable contribution to the humidity ratio increase for all four cities with a maximum increase from 1.7 g/kg to 4.9 g/kg in Inuvik.

Further work will focus on the energy impact of different defrost schedules and defrost threshold temperatures of ERV.

Acknolwedgements

References

[1]   D, R. International, Ltd., and under contract to P. N. N. Laboratory, "2011 Buildings Energy Data Book (U.S. Department of Energy) - Institute for Energy and Environmental Research.", accessed Jan. 20, 2021.

[2]   N. R. Canada, "R-2000: environmentally friendly homes," Feb. 02, 2018.

[3]   American Society of Heating, *1997 ASHRAE Handbook: Fundamentals.* Atlanta, GA: ASHRAE, 1997.

[4]   F. Steimle, J. Roben, "Ventilation requirements in modern buildings", *In Proceedings of the 13th AIVC conference Nice. France*, 414-422, 1992.

[5]   M. Justo Alonso, P. Liu, H. M. Mathisen, G. Ge, and C. Simonson, "Review of heat/energy recovery exchangers for use in ZEBs in cold climate countries," *Build. Environ.*, vol. 84, 228–237, Jan. 2015.

[6]   J. Zhang, A. S. Fung, "Experimental and numerical investigation of the thermal impact of defrost cycle of residential heat and energy recovery ventilators," *Energy Build.*, vol. 97, 129–136, Jun. 2015.

[7]   P. Liu *et al.*, "A theoretical model to predict frosting limits in cross-flow air-to-air flat plate heat/energy exchangers," *Energy Build.*, vol. 110, 404–414, Jan. 2016.

[8]   C. Beattie, P. Fazio, R. Zmeureanu, and J. Rao, "Experimental study of air-to-air heat exchangers for use in arctic housing," *Appl. Therm. Eng.*, vol. 129, 1281–1291, Jan. 2018.

[9]   R. Östin, "A study of heat exchange under frosting conditions," *Heat Recovery Syst. CHP*, vol. 12, no. 2, 89–103, Mar. 1992.

[10]   D. W. Schulte and R. H. Howell, "The Effects of Air Turbulence on the rate of Frost Growth on a Horizontal Plate," *ASHRAE Trans.*, vol. 88, pt. 2, 201–217, 1982.

[11]   M. Rafati Nasr, M. Fauchoux, R. W. Besant, and C. J. Simonson, "A review of frosting in air-to-air energy exchangers," *Renew. Sustain. Energy Rev.*, vol. 30, 538–554, Feb. 2014.

[12]   W. J. Fisk, R. E. Chant, K. M. Archer, D. Hekmat, F. J. Offermann and B. S. Pedersen, "Performance of residential air-to-air heat exchangers during operation with freezing and periodic defrosts," *ASHRAE Trans.*, vol. 91, pt.1, 159-172, 1985.

[13]   E. G. Phillips, R. E. Chant, B. C. Bradley and D. R. Fisher. "A model to compare freezing control strategies for residential air-to-air heat recovery ventilators," *ASHRAE Trans.*, vol. 95, pt. 2, 454-483, 1989.

[14]   E. G. Phillips, D. R. Fisher, R. E. Chant, and B. C. Bradley, "Freeze-control strategy and air-to-air energy recovery performance," *ASHRAE J,* 44–49, Dec-1992.

[15]   "Frost-Control-Strategies-for-Airxchange-Wheels.pdf," Accessed: Jan. 16, 2021.

[16]   J. Y. Jang, H. H. Bae, S. J. Lee, and M. Y. Ha, "Continuous heating of an air-source heat pump during defrosting and improvement of energy efficiency," *Appl. Energy*, vol. 110, 9–16, Oct. 2013.

[17]   E. G. Phillips, L. C. Bradley, R. E. Chant, and D. R. Fisher, "Comparison of freezing control strategies for residential air-to-air heat recovery ventilators," *ASHRAE Trans.*, vol. 95, pt. 2, 890-609, Jun. 1989.

[18]   X.R. Zhang, L.Z. Zhang, H.M. Liu, and L.X. Pei, "One-step fabrication and analysis of an asymmetric cellulose acetate membrane for heat and moisture recovery," *J. Member. Sci.*, vol. 366, no. 1–2, 158–165, Jan. 2011.

[19]   P.T. Ninomura, R. Bhargava, "Heat recovery ventilators in multifamily residences in the arctic," *ASHRAE Trans.*, vol. 101, pt. 2, 14-97, 1995.

[20]   G. B. Davis, "Energy recovery ventilator: means for defrosting heat exchanger medium and damper motor actuation means," *US. Patent.*, vol 5, 497-823, 1996.

[21]   M. Leckner, R. Zmeureanu, "Life Cycle Cost and Energy Analysis of a Net Zero Energy House with Solar Combisystem," *Appl. Energy.*, vol. 88, 232-241, 2011.

[22]   "Weather Data | EnergyPlus.", accessed Nov. 21, 2020.

[23]   J.Zhang and A. S. Fung, "Experimental study and analysis of an energy recovery ventilator and the impacts of defrost cycle," *Energy Build*, vol. 87,265-271,Jan. 2015